Available online at www.sciencedirect.com
SCIENCE DIRECT®
International Journal of Heat and Mass Transfer 49 (2006) 2751–2761
International Journal of HEAT and MASS TRANSFER
www.elsevier.com/locate/ijhmt

Thermal analysis on metal-foam filled heat exchangers. Part I: Metal-foam filled pipes

W. Lu [a], C.Y. Zhao [a,b,*], S.A. Tassou [a]

[a] Department of Mechanical Engineering, School of Engineering and Design, Brunel University, Uxbridge, Middlesex, UB8 3PH, UK
[b] State Key Laboratory of Multiphase Flow and Heat Transfer, School of Energy and Power Engineering, Xi'an Jiaotong University, Shaanxi, 710049, PR China

Received 8 September 2005
Available online 10 March 2006

Abstract

This paper presents an analytical study of the forced convection heat transfer characteristics in high porosity open-cell metal-foam filled pipes. The Brinkman-extended Darcy momentum model and two-equation heat transfer model for porous media were employed. Based on the analytical solutions, the velocity and temperature distributions in metal-foam filled pipes were obtained. The effects of the microstructure of metal foams on overall heat transfer were examined. The results show that the pore size and porosity of metal-foams play important roles on overall heat transfer performance. The use of metal-foam can dramatically enhance the heat transfer but at the expense of higher pressure drop.

1. Introduction

As a new material, metal-foams are attracting increasing attention for a variety of applications. The advantages of metal-foams lie on their low-density, large surface area in a limited volume and high strength structure. Due to high manufacturing costs metal-foams have, until recently, mainly been used in the aerospace, ship-building and defence industries. More recently, the development of the metal sintering method for foam manufacture has led to decreasing manufacturing costs and an increasing range of applications including heat and mass transfer [1–7]. To effectively use metal-foam materials in heat exchange devices it is necessary to combine the material with tubes and sheets for flow separation and heat transfer. Development efforts have taken place at Porvair Fuel Cell Technology to successfully combine a variety of metal-foam materials with solid structures, and metal-foam filled tubes have also been manufactured. Data presented in this paper are based on metal-foams attached to the solid structure using a Porvair proprietary co-sintering technique.

The expanding range of applications is also leading to increased interest in the study of the thermal and transport phenomena in high porosity open-cell metal foams. Bhattacharya et al. [1] determined the thermo-physical properties of high porosity metal foams, such as effective thermal conductivity (k_e), permeability (K) etc., based on comprehensive analytical and experimental investigations. Boomsma and Poulikakos [2] developed an effective thermal conductivity model based on the idealized three-dimensional cell geometry of a foam which was validated experimentally. This was similar to the model proposed by Calmidi [3] and Calmidi and Mahajan [4] who performed experimental studies with a wide variety of aluminium foams. Zhao et al. [5,6] conducted experimental and numerical studies for air-cooling forced convection in FeCrAlY metal-foam filled plate channels. Zhao et al. [6] and Phanikumar and Mahajan [7] also presented numerical

* Corresponding author. Address: Department of Mechanical Engineering, School of Engineering and Design, Brunel University, Uxbridge, Middlesex, UB8 3PH, UK. Tel.: +44 01895266697/+86 02982668036.
E-mail addresses: chang-ying.zhao@Brunel.ac.uk, cyzhao@mail.xjtu.edu.cn (C.Y. Zhao).

0017-9310/$ - see front matter © 2006 Elsevier Ltd. All rights reserved.
doi:10.1016/j.ijheatmasstransfer.2005.12.012

Nomenclature

$\widetilde{a}$	surface area density (m^{-1})
c_p	heat capacity of fluid (J/kg K)
Da	Darcy number, K/R^2
d_f	diameter of the fibre of metal foams (m)
d_p	pore size (m)
f	friction factor
h	heat-transfer coefficient (W/m^2 K)
h_{sf}	interfacial heat-transfer coefficient of metal foams (W/m^2 K)
k	thermal conductivity (W/m K)
k_e	effective thermal conductivity (W/m K)
K	permeability (m^2)
Nu	Nusselt number, $2hR/k_f$
Nu_{sf}	local Nusselt number $h_{sf}d_p/k_f$
p	pressure (Pa)
P	dimensionless pressure
Pr	Prandtl number, $c_p\mu_f/k$
q_w	heat flux (W/m^2)
R	pipe radius (m)
Re	Reynolds number, $2uR/\upsilon$
Re_d	local Reynolds number, ud/υ
T	temperature (K)
u	velocity along z direction, V_z (m/s)
u_m	mean fluid velocity along z direction (m/s)
U	dimensionless velocity along z direction, u/u_m
$\vec{V}$	velocity vector

Greek symbols

ε	porosity
θ	dimensionless temperature, $\frac{T-T_w}{q_wR/k_{se}}$
Σ	sum
ρ	density (kg/m^3)
μ_f	dynamic viscosity (kg/m s)
υ	kinematic viscosity (m^2/s)
ψ	dimensionless radial coordinate, r/R

Subscripts

s	solid
f	fluid
w	wall

Others

$\langle\rangle$	volume averaged value
∇	total differential
∂	partial differential

and experimental results for Non-Darcy natural convection in high porosity metal foams.

In principle, high porosity metal-foams with open cells can be treated as a porous medium. Darcy [8] first summarised the correlation for the flow in porous media based on experimental observations. He discovered that the area-averaged fluid velocity through a column of porous material is proportional to the pressure gradient established along the column. Subsequent experiments proved that the area-averaged velocity is, in addition, inversely proportional to the viscosity (μ) of the fluid seeping through the porous material. For a one-dimensional forced flow, Darcy's law can be represented as $u = \frac{K}{\mu}\langle -\frac{dP}{dx}\rangle$, where K is an empirical constant called permeability.

Darcy's law, however, neglects the viscous force acting along the impermeable surface (solid boundary) and for this reason, when the Reynolds number based on the pore diameter for the channel/pipe flows exceeds 1–10, significant deviations from test results were found [9]. To solve this problem, the Brinkman-extended Darcy model [10] was proposed to consider the effect of the impermeable boundary, and has since been extensively used for non-Darcy flows [11–13]. Zhao and Lu [11] and Kim et al. [12] both used the Brinkman-extended Darcy model for the analyses of channel heat sinks. Nazar et al. [13] applied the model for the theoretical study of the mixed convective boundary layer flow past a horizontal circular cylinder embedded in a porous medium. In the present study, the Brinkman-extended Darcy model is employed as the momentum equation to analyse the velocity distribution in metal-foam filled pipes.

For modelling the heat transfer in a porous medium, the one-equation equilibrium model or the two-equation non-equilibrium model are commonly used [8]. The one-equation equilibrium model assumes that there is no temperature difference between the local fluid and solid phase while the two-equation non-equilibrium model treats the fluid and solid separately, considering the local temperature difference between them. The latter is more difficult to apply because it requires information on the interfacial heat-transfer coefficient, which is usually determined through experimental investigations. Owing to this difficulty, some investigators have used the one-equation model for the analysis of convection heat transfer in a general porous medium [13]. However, the one equation model is only valid when the local temperature difference between fluid and solid is negligibly small. This will not be the case in heat exchanger applications where the difference in the thermal conductivities of the fluid and solid is significant [4,5] and for this reason the two-equation non-equilibrium heat transfer model is used to study the heat transfer performance of metal-foam filled pipes. To obtain the interfacial heat-transfer coefficient of open-cell metal foams, the correlation based on a three-dimensional cross-cylinder representation [14] will be employed.

Although, as indicated above, some investigations of heat transport in open-cell metal-foams have been carried out the work has mainly concentrated on metal-foam plate

Fig. 1. Metal-foam filled tubes using co-sintering technique.

channels. No work has been presented, as yet, in the open literature on metal-foam filled pipe flows and associated heat exchangers, which have significant potential applications in industry.

This paper presents an analytical study of forced flow heat transfer in metal-foam filled pipes (shown in Fig. 1). It provides details of the analytical method used to solve the momentum and energy equations and presents results for velocity and temperature distribution and pressure drop. A parametric analysis is also presented and the analytical results are compared with experimental data. The performance of a metal-foam filled tube heat exchanger is analysed in the companion paper II.

2. Physical problem

The problem under consideration is forced convective flow through a metal-foam filled pipe, as shown in Fig. 2. The diameter of the pipe is $2R$, and the length of the tube is L. The wall of the pipe is uniformly heated and the fluid (such as water or air) is assumed to flow through the open-cell metal-foam filled area, removing heat from the wall of the pipe without phase change.

3. Mathematical formulations and their analytical solutions

3.1. Mathematical formulations

As mentioned earlier, the momentum equation employed is based on the Brinkman-extended Darcy model [10] and the energy equations for both fluid and solid used, are based on the two-equation non-equilibrium heat transfer model proposed by Calmidi and Mahajan [4]. These are detailed below:

- Mass conservation equation

$$\nabla(\rho\vec{V}) = 0. \tag{1}$$

- Momentum equation (Brinkman–Darcy model)

$$\frac{1}{\varepsilon}\langle(\vec{V}\cdot\nabla)\rho_{\mathrm{f}}\vec{V}\rangle = -\nabla\langle p\rangle_{\mathrm{f}} + \frac{\mu_{\mathrm{f}}}{\varepsilon}\nabla^2\langle\vec{V}\rangle - \frac{\mu_{\mathrm{f}}}{K}\langle\vec{V}\rangle. \tag{2}$$

$\langle\ \rangle$ means a volume averaged value.

- Energy balance equations for the solid and fluid

$$0 = \nabla\cdot\{k_{\mathrm{se}}\nabla\langle T_{\mathrm{s}}\rangle\} - h_{\mathrm{sf}}\tilde{a}(\langle T_{\mathrm{s}}\rangle - \langle T_{\mathrm{f}}\rangle), \tag{3}$$

$$\langle\rho\rangle_{\mathrm{f}}C_{\mathrm{f}}\langle\vec{V}\rangle\nabla T_{\mathrm{f}} = \nabla\cdot\{(k_{\mathrm{fe}}+k_{\mathrm{d}})\cdot\nabla\langle T_{\mathrm{f}}\rangle\} + h_{\mathrm{sf}}\tilde{a}(\langle T_{\mathrm{s}}\rangle - \langle T_{\mathrm{f}}\rangle). \tag{4}$$

In Eq. (2), $\vec{V}$ is the velocity vector, ε is the porosity of the porous medium, p is the pressure, μ_{f} is the fluid viscosity and K is the permeability of the porous medium. In Eq. (3), $\tilde{a}$ is the surface area density of the metal-foam and h_{sf} is the interfacial heat-transfer coefficient between the solid surface and the fluid. C_{f} and ρ_{f} are the heat capacity and density of fluid respectively, whereas k_{se} and k_{fe} are the effective thermal conductivities of solid and fluid.

In the analysis it is assumed that the flow is both hydraulically and thermally fully developed. All thermophysical properties of the solid and fluid, e.g., thermal conductivity, density, specific heat and viscosity, are assumed to be temperature independent. Natural convection and radiation are negligible. The porous medium is assumed homogeneous and isentropic, and thus the problem can be considered axially symmetrical. In addition, Calmidi and Mahajan [4] and Phanikumar and Mahajan [7] concluded from their studies that the enhancing effect of thermal dispersion (k_{d}) is extremely low due to the relatively high conductivity of the solid matrix. Therefore, The term k_{d} is dropped to simplify the analysis. Due to the assumption of fully developed flow, the equation $\frac{\partial T_{\mathrm{w}}}{\partial z} = \frac{\partial T_{\mathrm{f}}}{\partial z} = \frac{\partial T_{\mathrm{s}}}{\partial z} = \text{const}$ holds. Based on these assumptions, Eqs. (1)–(4) can be simplified as follows:

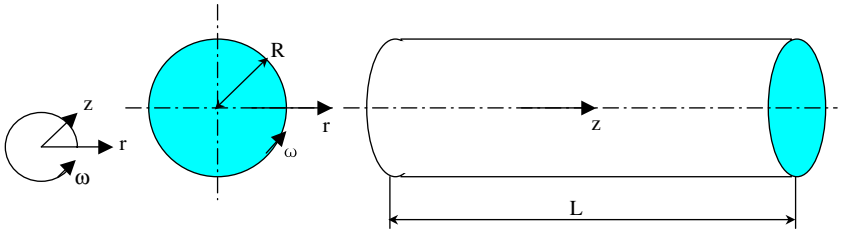

Fig. 2. Schematic diagram of a metal-foam filled pipe.

$$0 = -\frac{\mathrm{d}p}{\mathrm{d}z} + \frac{\mu_\mathrm{f}}{\varepsilon}\left(\frac{\partial^2 u}{\partial r} + \frac{1}{r}\frac{\partial u}{\partial r}\right) - \frac{\mu_\mathrm{f}}{K}u, \tag{5}$$

$$0 = k_\mathrm{se}\left(\frac{\partial^2 T_\mathrm{s}}{\partial r^2} + \frac{1}{r}\frac{\partial T_\mathrm{s}}{\partial r}\right) - h_\mathrm{sf}\tilde{a}(T_\mathrm{s} - T_\mathrm{f}), \tag{6}$$

$$\varepsilon\rho_\mathrm{f}C_\mathrm{f}u\frac{\mathrm{d}T_\mathrm{f}}{\mathrm{d}z} = k_\mathrm{fe}\cdot\left(\frac{\partial^2 T_\mathrm{f}}{\partial r^2} + \frac{1}{r}\frac{\partial T_\mathrm{f}}{\partial r}\right) + h_\mathrm{sf}\tilde{a}(T_\mathrm{s} - T_\mathrm{f}), \tag{7}$$

where brackets $\langle\ \rangle$ are dropped for simplicity, and u is the velocity along the z direction, V_z.

For the metal-foam filled pipes directly heated from outside surface with constant heat flux, the applied heat is transferred to the solid and fluid phases by conduction and convection. As discussed by Zhao et al. [14] and Lee and Vafai [15], because the thermal conductivity of the thin metal wall of pipe is significantly higher than that of the fluid the temperature at the interface between the metal-foam and the substrate can be considered to be uniform regardless of whether it is in contact with the solid or fluid. Consequently, the boundary conditions of metal-foam filled pipe can be specified as follows:

$$\text{When } r = R, \quad u = 0, \quad T_\mathrm{s} = T_\mathrm{f} = T_\mathrm{w}, \tag{8}$$

$$\text{When } r = 0, \quad \frac{\partial u}{\partial r} = \frac{\partial T_\mathrm{f}}{\partial r} = \frac{\partial T_\mathrm{s}}{\partial r} = 0, \tag{9}$$

where T_w implies the temperature at the interface. This temperature is not known a priori and must be obtained as part of the solution.

To proceed further, there are parameters in the above equations that need to be established. They are permeability (K), effective thermal conductivities of the solid and fluid phases (k_se and k_fe), surface area density ($\tilde{a}$) and the interfacial heat-transfer coefficient (h_sf).

- Permeability (K)
  The permeability (K) of metal-foams, which is the key parameter for solving the momentum equation, has been investigated by several researchers. Calmidi [3] proposed a specific formulation for K based on experimental data.

$$\frac{K}{d_\mathrm{p}^2} = 0.00073(1-\varepsilon)^{-0.224}(d_\mathrm{f}/d_\mathrm{p})^{-1.11}, \tag{10}$$

  where d_p is the pore size ($d_\mathrm{p} = 0.0254/\text{ppi}$ meter, ppi: pores per inch), d_f is the fibre diameter of metal-foams $\left(\frac{d_\mathrm{f}}{d_\mathrm{p}} = 1.18\sqrt{\frac{(1-\varepsilon)}{3\pi}}\left(\frac{1}{1-e^{-((1-\varepsilon)/0.04)}}\right)\right)$ [5].

- Effective thermal conductivities of the solid and fluid (k_se and k_fe)
  To determine the effective thermal conductivity of open-cell metal foams, k_e, the following correlation, which is based on the three-dimensional cellular morphology, was proposed by Boomsma and Poulikakos [2].

$$k_\mathrm{e} = \frac{\sqrt{2}}{2(R_A + R_B + R_C + R_D)}, \tag{11}$$

where

$$R_A = \frac{4\lambda}{(2e^2 + \pi\lambda(1-e))k_\mathrm{s} + (4 - 2e^2 - \pi\lambda(1-e))k_\mathrm{f}},$$

$$R_B = \frac{(e-2\lambda)^2}{(e-2\lambda)e^2k_\mathrm{s} + (2e - 4\lambda - (e-2\lambda)e^2)k_\mathrm{f}},$$

$$R_C = \frac{(\sqrt{2}-2e)^2}{2\pi\lambda^2(1-2e\sqrt{2})k_\mathrm{s} + 2(\sqrt{2} - 2e - \pi\lambda^2(1-2e\sqrt{2}))k_\mathrm{f}},$$

$$R_D = \frac{2e}{e^2k_\mathrm{s} + (4-e^2)k_\mathrm{f}},$$

where $\lambda = \sqrt{\frac{\sqrt{2}(2-(5/8)e^3\sqrt{2}-2\varepsilon)}{\pi(3-4e\sqrt{2}-e)}}$, $\quad e = 0.339$.

  After the overall effective thermal conductivity is obtained, the effective solid conductivity, k_se, can be established by setting $k_\mathrm{f} = 0$. Similarly, the effective fluid conductivity, k_fe, can be determined by setting $k_\mathrm{s} = 0$.

- Surface area density ($\tilde{a}$)
  The solid–fluid interfacial surface area density for an array of parallel cylinders intersecting in three mutually perpendicular directions, whose cylinder diameter is d and interval is a, is $\frac{3\pi d}{a^2}$. However, the topology of metal-foams is different from the cross-cylinder. Furthermore, the cross-section of the fibre is not circular when the porosity of metal-foams is higher than 0.85. Shape factors must be introduced when the formula of cross-cylinder is used to simplify the structure of metal-foams, which are $a = 0.59d_\mathrm{p}$, and $d = (1 - \mathrm{e}^{-((1-\varepsilon)/0.04)})\cdot d_\mathrm{f}$ [3]. Then the surface area density of metal-foams becomes

$$\tilde{a} = \frac{3\pi d_\mathrm{f}(1 - \mathrm{e}^{-((1-\varepsilon)/0.04)})}{(0.59d_\mathrm{p})^2}. \tag{12}$$

- The interfacial heat-transfer coefficient (h_sf)
  The interfacial heat-transfer coefficient for packed beds is usually calculated using a correlation proposed by Wakao et al. [16]. However, no such general correlation exists for metal-foams. So the following correlation developed by Zukauskas [17], which is valid for staggered cylinders, is used to estimate h_sf

$$Nu_\mathrm{sf} = \frac{h_\mathrm{sf}d}{k_\mathrm{f}} = \begin{cases} 0.76Re_\mathrm{d}^{0.4}Pr^{0.37}, & (10^0 \leqslant Re_\mathrm{d} \leqslant 4\times10^1), \\ 0.52Re_\mathrm{d}^{0.5}Pr^{0.37}, & (4\cdot10^1 \leqslant Re_\mathrm{d} \leqslant 10^3), \\ 0.26Re_\mathrm{d}^{0.6}Pr^{0.37}, & (10^3 \leqslant Re_\mathrm{d} \leqslant 2\times10^5), \end{cases} \tag{13}$$

  where Re_d is the local Reynolds number, $Re_\mathrm{d} = ud/v$. For metal foams, as discussed above, the cross-section of the fibres is not circular and to account for this the shape factor, $d = (1 - \mathrm{e}^{-((1-\varepsilon)/0.04)})\cdot d_\mathrm{f}$, is introduced.

3.2. Normalisation of equations

Equations and boundary conditions can be non-dimensionalised by introducing the following dimensionless variables:

$$Da = K/R^2, \quad \psi = r/R, \quad P = \frac{K}{\mu_f u_m}\frac{dp}{dz}, \quad \theta = \frac{T - T_w}{q_w R/k_{se}},$$
$$\theta_s = \frac{T_s - T_w}{q_w R/k_{se}}, \quad \theta_f = \frac{T_f - T_w}{q_w R/k_{se}}, D = h_{sf}\tilde{a}R^2/k_{se},$$
$$C = \frac{k_{fe}}{k_{se}}, \quad U = \frac{u}{u_m}, \tag{14}$$

where q_w is the heat flux over the surface of the pipe and u and u_m are the local velocity and mean velocity along the axial direction, respectively.

For fully developed flow subject to a constant heat flux, the dimensionless equations and boundary conditions can be expressed as follows.

- The dimensionless momentum equation:

$$U = -P + \frac{Da}{\varepsilon}\left(\frac{\partial^2 U}{\partial\psi} + \frac{1}{\psi}\frac{\partial U}{\partial\psi}\right). \tag{15}$$

- The dimensionless energy balance equations for the solid and fluid:

$$0 = \frac{\partial^2\theta_s}{\partial\psi^2} + \frac{1}{\psi}\frac{\partial\theta_s}{\partial\psi} - D(\theta_s - \theta_f), \tag{16}$$

$$2U = C\cdot\left(\frac{\partial^2\theta_f}{\partial\psi^2} + \frac{1}{\psi}\frac{\partial\theta_f}{\partial\psi}\right) + D(\theta_s - \theta_f). \tag{17}$$

- The dimensionless boundary conditions are:

$$U = \theta_s = \theta_f = 0 \quad \text{at } \psi = 1, \tag{18}$$

$$\frac{dU}{d\psi} = \frac{\partial\theta_s}{\partial\psi} = \frac{\partial\theta_f}{\partial\psi} = 0 \quad \text{at } \psi = 0. \tag{19}$$

3.3. Analytical solution of the equations

The above equations can be treated as equations of the form $\frac{\partial^2 Y}{\partial z^2} + \frac{1}{z}\frac{\partial Y}{\partial z} - Y = 0$ and $\frac{\partial^2 Y}{\partial z^2} + \frac{1}{z}\frac{\partial Y}{\partial z} = C$. The latter is easy to solve. The standard solutions of the former, $J_0(z)$ and $Y_0(z)$ are given in the Appendix. Based on these, Eqs. (15)–(17) can be analytically solved under boundary conditions (18) and (19).

3.4. Dimensionless velocity distributions

The velocity distribution can be obtained by solving the momentum Eq. (15), as

$$U = P\frac{J_0\left(\sqrt{\frac{\varepsilon}{Da}}\psi\right)}{J_0\left(\sqrt{\frac{\varepsilon}{Da}}\right)} - P. \tag{20}$$

From the continuum equation the following relationship is valid $\frac{1}{A}\int_A U\,dA = 1$, namely,

$$\frac{1}{\pi}\int_0^{2\pi}\int_0^1 P\left(J_0\left(\sqrt{\frac{\varepsilon}{Da}}\psi\right)\Big/ J_0\left(\sqrt{\frac{\varepsilon}{Da}}\right)\right)\psi\,d\psi\,d\theta = 1.$$

Hence

$$P = \frac{J_0\left(\sqrt{\frac{\varepsilon}{Da}}\right)}{2\sqrt{\frac{Da}{\varepsilon}}J_1\left(\sqrt{\frac{\varepsilon}{Da}}\right) - J_0\left(\sqrt{\frac{\varepsilon}{Da}}\right)}. \tag{21}$$

From Eq. (14), a formulation for the pressure drop can be deduced as

$$\frac{dp}{dz} = \frac{\mu_f u_m}{K}P. \tag{22}$$

Integrating both sides, Eq. (22) becomes

$$\Delta p = \int_0^L \frac{\mu_f u_m}{K}P\,dz = \frac{\mu_f u_m}{K}PL. \tag{23}$$

Finally, the friction factor is given by

$$f = \frac{\Delta\langle p\rangle 2R}{L\rho_f u_m^2/2} = \frac{4\mu_f}{K\rho_f u_m}P\cdot R = \frac{8P}{Da\cdot Re}. \tag{24}$$

3.5. Dimensionless temperature distributions

After the velocity distribution is determined, the temperature profile can be obtained from the solution of Eqs. (16) and (17).

$$\theta_s = 2P\left(-\frac{1}{4}\psi^2 + \frac{\frac{Da}{\varepsilon}}{J_0\left(\sqrt{\frac{\varepsilon}{Da}}\right)}J_0\left(\sqrt{\frac{\varepsilon}{Da}}\psi\right) + \frac{1}{4} - \frac{Da}{\varepsilon}\right) - C\theta_f \tag{25}$$

$$\theta_f = \frac{2P}{C+1}\left(-\frac{1}{4}\psi^2 + \frac{\frac{Da}{\varepsilon}}{J_0\left(\sqrt{\frac{\varepsilon}{Da}}\right)}J_0\left(\sqrt{\frac{\varepsilon}{Da}}\psi\right) + \frac{1}{4} - \frac{Da}{\varepsilon} - B\cdot\frac{1}{J_0\left(\sqrt{\frac{(C+1)D}{C}}\right)}\cdot J_0\left(\sqrt{\frac{(C+1)D}{C}}\psi\right) + A\cdot\frac{1}{J_0\left(\sqrt{\frac{\varepsilon}{Da}}\right)}J_0\left(\sqrt{\frac{\varepsilon}{Da}}\psi\right) + \frac{1}{(C+1)\cdot D}\right), \tag{26}$$

where $A = \frac{1}{(C\cdot\frac{\varepsilon}{Da} - (C+1)\cdot D)}$ and $B = \frac{C\cdot\frac{\varepsilon}{Da}}{(C+1)\cdot D\cdot(C\cdot\frac{\varepsilon}{Da} - (C+1)\cdot D)}$. Therefore, $B - A = \frac{1}{(C+1)\cdot D}$.

3.6. Heat transfer performance

From the analytical solutions for velocity and temperature distributions, the overall Nusselt number of a metal-foam filled pipe can be determined as

$$Nu = \frac{\bar{h}}{k_f}2R = \frac{2Rq_w}{k_f(T_w - T_{f,b})} = -\frac{2k_{se}}{k_f\theta_{f,b}} = -\frac{2}{(k_f/k_{fe})\cdot C\theta_{f,b}}, \tag{27}$$

where $\bar{h}$ is the overall heat-transfer coefficient between the surface and the fluid based on the bulk-mean temperature and $\theta_{f,b}$ is the dimensionless bulk-mean fluid temperature averaged along the cross-section of the channel, given by

$$\theta_{f,b}=\frac{T_{f,b}-T_w}{q_w R/k_{se}}=\frac{\int_0^{2\pi}\int_0^1 U\theta_f\psi\,d\psi\,d\vartheta}{\int_0^{2\pi}\int_0^1 U\psi\,d\psi\,d\vartheta}=2\int_0^1 U\theta_f\psi\,d\psi$$
$$=\frac{4P^2}{C+1}\left(\left(A+\frac{Da}{\varepsilon}\right)\int_0^1\left(\frac{J_0\left(\sqrt{\frac{\varepsilon}{Da}}\psi\right)}{J_0\left(\sqrt{\frac{\varepsilon}{Da}}\right)}\right)^2\psi\,d\psi\right.$$
$$-B\int_0^1\frac{J_0\left(\sqrt{\frac{(C+1)D}{C}}\psi\right)}{J_0\left(\sqrt{\frac{(C+1)D}{C}}\right)}\frac{J_0\left(\sqrt{\frac{\varepsilon}{Da}}\psi\right)}{J_0\left(\sqrt{\frac{\varepsilon}{Da}}\right)}\psi\,d\psi$$
$$-\frac{1}{4}\int_0^1\frac{J_0\left(\sqrt{\frac{\varepsilon}{Da}}\psi\right)}{J_0\left(\sqrt{\frac{\varepsilon}{Da}}\right)}\psi^3\,d\psi-\left(2A+2\frac{Da}{\varepsilon}-B-\frac{1}{4}\right)$$
$$\times\frac{J_1\left(\sqrt{\frac{\varepsilon}{Da}}\right)}{J_0\left(\sqrt{\frac{\varepsilon}{Da}}\right)}\sqrt{\frac{Da}{\varepsilon}}+B\frac{J_1\left(\sqrt{\frac{(C+1)D}{C}}\right)}{J_0\left(\sqrt{\frac{(C+1)D}{C}}\right)}\sqrt{\frac{C}{(C+1)D}}$$
$$\left.+\frac{1}{2}\left(A+\frac{Da}{\varepsilon}-B-\frac{1}{8}\right)\right). \quad (28)$$

From the above analytical solutions, it can be seen that the non-dimensional velocity (U) is a function of $\sqrt{\frac{\varepsilon}{Da}}$. Similarly, the non-dimensional temperatures (θ_s and θ_f) and the overall Nusselt number ($Nu=\frac{\bar{h}}{k_f}2R$) of metal-foam filled pipes are the functions of $\sqrt{\frac{\varepsilon}{Da}}$, $\sqrt{\frac{(C+1)D}{C}}$, and C. From the above Eqs. (10)–(14), the following results can be deduced, as

$$\sqrt{\frac{\varepsilon}{Da}}=f_1(\varepsilon)\frac{R}{d_p}, \quad (29)$$

$$\sqrt{\frac{(C+1)D}{C}}=f_2(\varepsilon)((C+1)Re_d^n Pr^{0.37})^{1/2}\frac{R}{d_p}, \quad (30)$$

and

$$C=\frac{k_{fe}}{k_{se}}=f_c(\varepsilon)\frac{k_f}{k_s}, \quad (31)$$

where $Re_d=\frac{Re\cdot d}{2R}=0.5Re\frac{d_p}{R}\frac{d_f}{d_p}(1-e^{-((1-\varepsilon)/0.04)})=0.5Re\frac{d_p}{R}f_d(\varepsilon)$, $f_1(\varepsilon)$, $f_2(\varepsilon)$, $f_d(\varepsilon)$, and $f_c(\varepsilon)$ are all a function of porosity (ε). Therefore, the heat transfer performance depends on four dimensionless parameters, R/d_p (geometry parameter), ε (porosity of metal foam), Re (Reynolds number, $2uR/v$) and k_f/k_s (fluid–solid thermal conductivity ratio).

4. Results and discussion

4.1. Velocity distributions

From the analytical solutions, it is shown that the non-dimensional velocity distribution (u/u_m), varies with R/d_p (geometry parameter) and ε (porosity of metal foam). Fig. 3 shows the velocity distribution in metal-foam filled pipes of different geometries and pore sizes. It can be seen that the metal foam can homogenize the flow compared to hollow channel flows, and the boundary layer becomes thinner with the increase of the ratio of tube diameter to pore size (R/d_p).

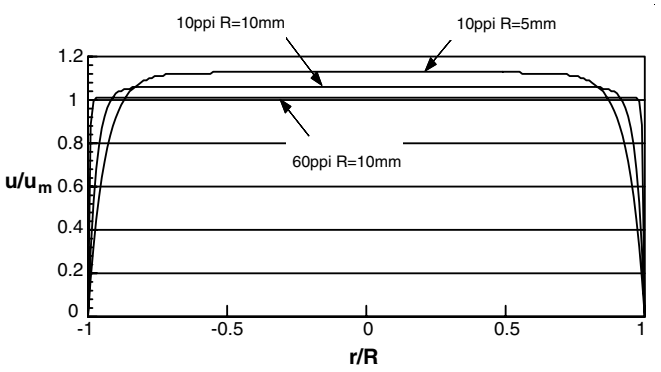

Fig. 3. Dimensionless velocity distribution in different metal-foam filled pipes ($\varepsilon=0.9$).

4.2. Pressure drop

This section considers the effect of different parameters on pressure drop along the length of the pipe. From Eq. (23), the pressure drop is a function of permeability (K) of the metal foam which in turn depends on the pore density (ppi) and porosity (ε). Consequently, the pressure drop of single-phase flow through the pipe increases exponentially with pore density (i.e. the decrease of pore size), as shown in Fig. 4. It is noted that the pressure drop of air through two pipes of different diameters but the same pore density is almost identical indicating that the pressure drop is mainly caused by the solid structure of the metal foam rather than the pipe wall. Fig. 5 shows the variation of pressure drop with the porosity at selected pore densities. As expected, the pressure drop increases with the decrease of porosity and increase in the pore density.

4.3. Temperature distribution

From the analytical solutions, it is observed that the solid and fluid temperature ($T-T_w/q_w$) distributions vary with $1/d_p$ (pore density), R (pipe radius), ε (porosity of metal foams), Re (Reynolds number), k_f and k_s (fluid and

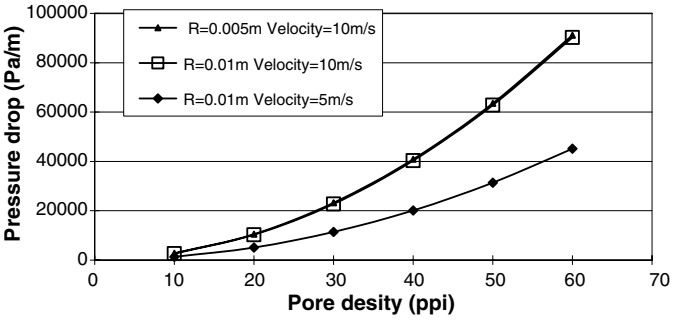

Fig. 4. Pressure drop per unit length along metal-foam filled pipes (porosity = 0.9).

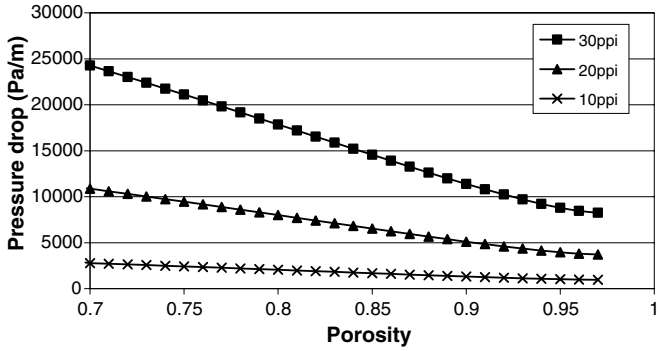

Fig. 5. Variation of pressure drop with porosity ($R = 0.01$ m, velocity = 5 m/s).

solid thermal conductivities). Figs. 6 and 7 show the effects of pore density and porosity on solid and fluid temperature distributions in metal-foam filled pipes, respectively.

Fig. 6 presents both the solid and fluid temperature distributions at selected pore densities (ppi). The pore density has a lower effect on the solid temperature distribution compared to the fluid temperature distribution. The temperature difference between the solid and fluid decreases sharply as the pore density (ppi) increases. With all other parameters constant, the increase of pore density leads to an increase in the wetted area available for the heat transfer between the solid and fluid phases. This leads to a higher local heat-transfer coefficient as well as a higher interfacial surface density (shown in Eq. (12)). Both are responsible for the reduction of the temperature difference between the solid and fluid.

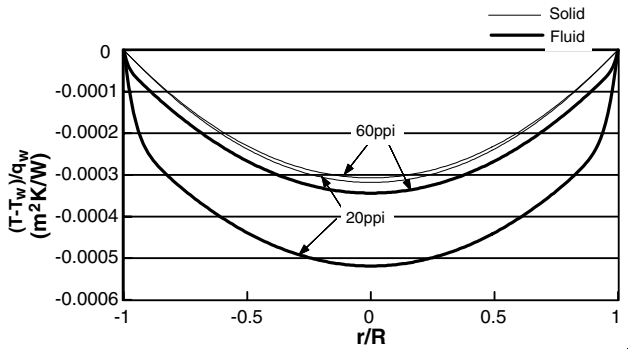

Fig. 6. Effect of pore density (ppi) on temperature distribution in metal-foam filled pipes (porosity = 0.9).

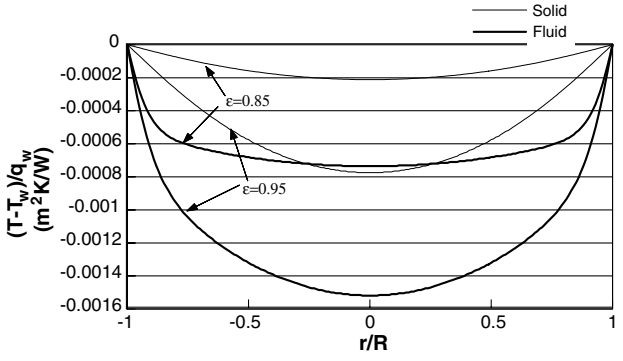

Fig. 7. Effect of porosity (ε) on temperature distribution in metal-foam (10 ppi) filled pipes.

Fig. 7 reveals that the variation of the porosity of metal-foams has a significant effect on both solid and fluid temperature distributions. As shown in this figure, the solid and fluid temperatures decrease much more quickly from the heated surface to the centre as the porosity of the metal-foam increases from 85% to 95%, while the temperature difference between the solid and fluid reduces slightly.

4.4. Overall heat transfer in metal-foam filled pipes

To examine the heat transfer rate between the heated wall and the fluid, the overall Nusselt number, defined as $Nu = \frac{\bar{h}}{k_f} 2R$, was used (Eq. (27)). From the analytical solutions, it is shown that the Nusselt number depends on four parameters: ε (porosity), R/d_p (geometry parameter), k_f/k_s (fluid–solid thermal conductivity ratio) and Re (Reynolds number). Figs. 8–13 present the effects of these parameters on the overall heat transfer coefficient (Nusselt number) for metal- foam filled pipes.

4.4.1. Effect of porosity

Fig. 8 shows the effect of porosity on the overall heat transfer coefficient. The Nusselt number increases gradually with the decrease of porosity, as expected. For a given

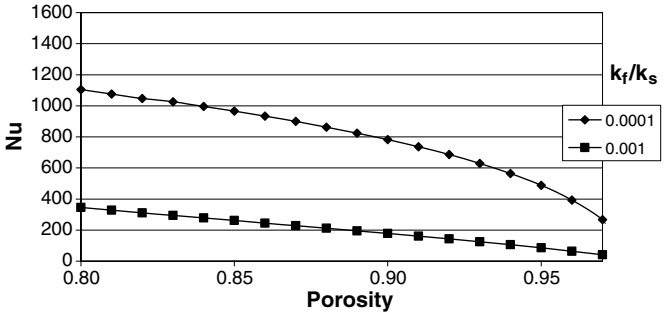

Fig. 8. Effect of porosity (ε) on overall Nusselt number for selected fluid-solid thermal conductivity ratios.

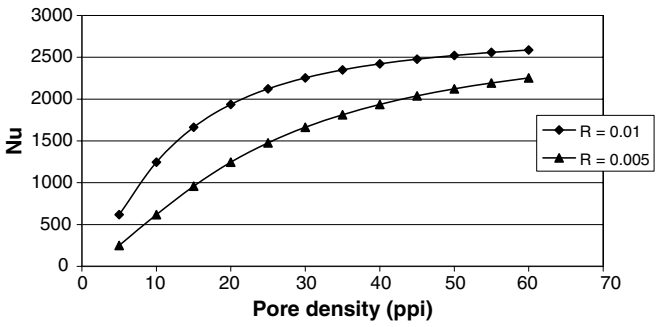

Fig. 9. Effect of pore density on overall Nusselt number for selected pipe sizes.

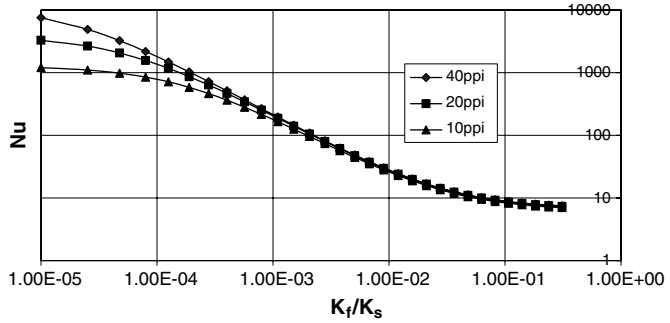

Fig. 10. Effect of k_f/k_s on overall Nusselt number in metal-foam ($\varepsilon = 0.9$) filled pipes at selected pore densities.

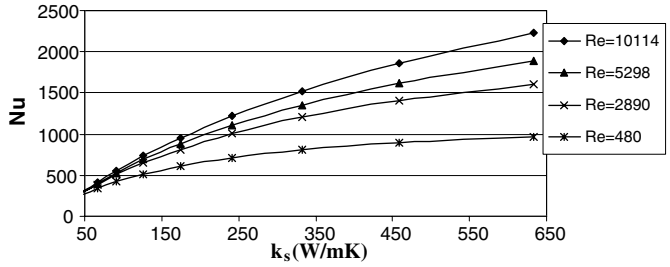

Fig. 11. Variation of Nusselt number with solid thermal conductivity (k_s) for air flowing through metal-foam filled pipes.

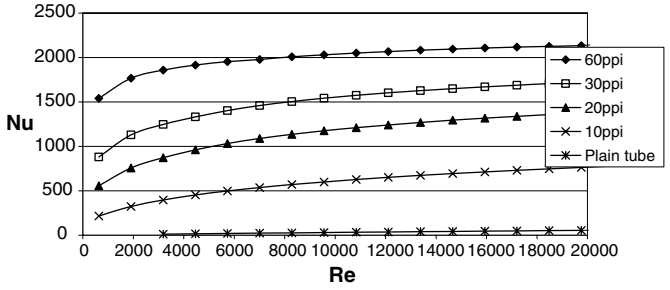

Fig. 12. Variation of Nusselt number with Reynolds number ($R = 0.005$ m, porosity $= 0.9$) for air flowing through metal-foam filled pipes.

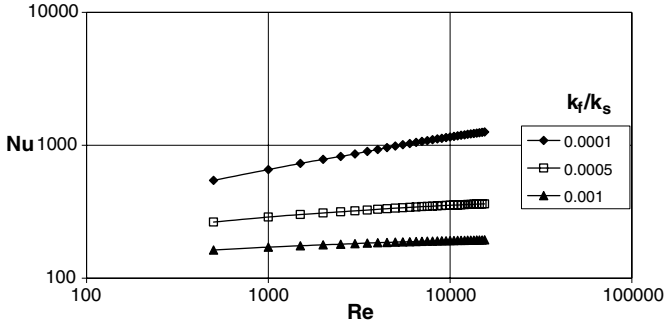

Fig. 13. *Nu–Re* diagram for metal-foam filled pipes at selected thermal conductivity ratios.

pore density (ppi), the fibre diameter and associated effective thermal conductivity increase with decreasing porosity.

4.4.2. Effect of pore size

It is shown in Fig. 9 that the effect of pore size ($d_p = 0.0254$/ppi meter) on heat transfer is significant. The Nusselt number sharply increases when pore density (ppi) increases, i.e. pore size decreases. For a given porosity, when the pore size decreases, the fibre diameter decreases correspondingly. This enlarges the interfacial surface density, which in turn enhances heat transfer from the metal-foam to the fluid. However, as shown in Figs. 10–12, the effect of pore density on the overall heat transfer coefficient varies with different fluid/solid conductivity ratio (k_f/k_s). From Fig. 10, it is evident that the pore density (ppi) has a very limited effect on Nusselt number when k_f/k_s is larger than 0.001.

4.4.3. Effect of thermal conductivity ratio

When the solid thermal conductivity is close to that of the fluid ($k_f/k_s > 0.1$), as shown in Fig. 10, the use of metal-foams has little effect on overall heat transfer. When $k_f/k_s < 0.1$, the overall heat transfer (Nusselt number) rises significantly with the increase of the solid thermal conductivity k_s, (see Fig. 11) and decrease of k_f/k_s down to a value of 0.00001. At relatively high values of k_f/k_s above 0.001, the pore density has very little effect on the Nusselt number which implies that the main thermal resistance is that of heat conduction through the solid fibres. At values of k_f/k_s below 0.001, the Nusselt number increases with pore density, indicating that the thermal resistance of the fluid begins to become significant.

4.4.4. Effect of Reynolds number

In this section, the effect of Reynolds number, $Re = u2R/v$, on heat transfer and temperature distribution is examined. As shown in Figs. 11–13, the overall heat transfer (Nusselt number) will rise with the increase in Reynolds number. The increased Reynolds number leads to a higher local heat-transfer coefficient, and in turn this enhances the heat transfer between the solid and fluid.

From the above results, it can be concluded that the overall heat transfer coefficient in metal-foam filled pipes depends on both the conduction heat transfer through the solid fibres of the metal-foam and convection heat transfer from the solid (fibres and wall) to the fluid. In other words, the overall thermal resistance can be divided into two parts, thermal resistance of solid and that of the fluid. The former is related to the porosity of the metal-foam, the diameter of pipe and the thermal conductivity of the foam. The latter is influenced by the properties of the fluid and interface area between solid and fluid. The increase of relative density (=1-porosity) and pore density of metal foams can greatly increase the conduction area of the solid fibres and the convection heat-transfer area, thereby reducing thermal resistance and enhancing the overall heat transfer. Therefore, in order to effectively

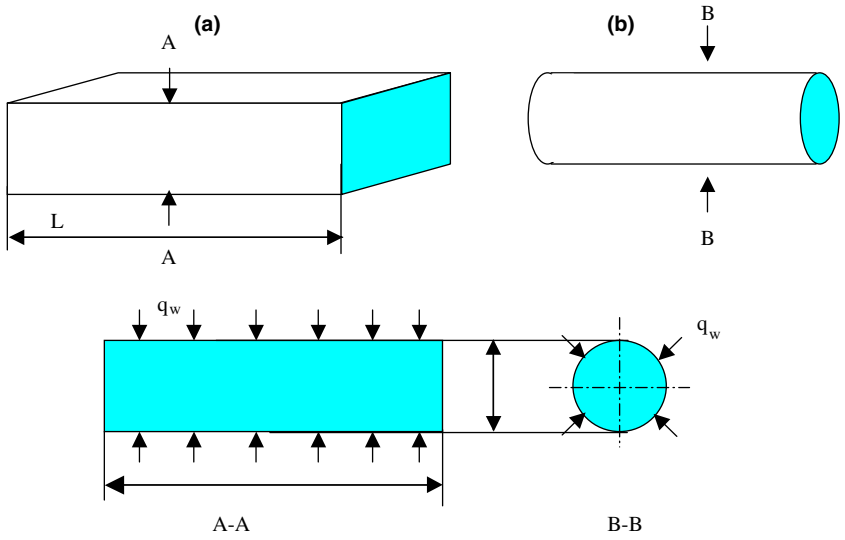

Fig. 14. (a) The tested plate channels in the experimental study and (b) the pipe analysed in this work. (A–A) and (B–B) are cross-sections of the test channel and pipe (all dimensions are in mm).

improve the overall heat transfer performance, the controlling thermal resistance between the metal-foam and fluid needs to be identified and minimised.

4.5. Comparison with experimental data

No experimental data has been published in the open literature, as yet, for heat transfer in metal-foam filled pipes. However, some experimental results are available for channel flows. Zhao et al. [5,14] conducted experimental studies for steel alloy (FeCrAlY) and copper foam channels. The channel width was ten times the channel height, so essentially the study could be considered two-dimensional with the channel height being the length scale that characterized the heat transfer behavior. This section presents a comparison between experimental results for the channel section and analytical results for the pipe section shown in Fig. 14. To make the comparison physically meaningful, both the plate channel and the pipe were assumed to have been filled with the same metal foam. The contact thermal resistance was taken into account through the experimental determination of the thermal conductivity of the metal-foam samples used in the investigation [5]. Modeling therefore took it into account by using relevant thermal conductivity for each sample. The diameter of the metal-foam filled pipe was also set to be equal to the height of plate channels thereby having the same characteristic length. The tested plate channels were uniformly heated from both bottom and top surfaces, whilst the pipes were assumed to have been uniformly heated from the outside surface.

To widen the range of comparison, two groups of samples were chosen. One was made of copper and the other from steel alloy FeCrAlY. The details of properties of each sample are given in Table 1. Fig. 15 shows a comparison between the analytical results for pipe flows and experimental data for channel flows. It can be seen that for all samples modeling and experimental results exhibit very similar trends. The heat transfer coefficients obtained from

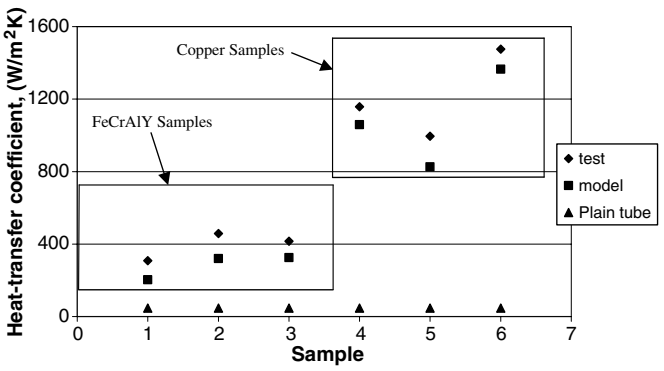

Fig. 15. Heat-transfer coefficient for different samples: analytical modeling versus test results [5,14].

Table 1
Summary of microstructures and thermal conductivities of compared samples [5]

Sample	s-1	s-2	s-3	s-4	s-5	s-6
Foam	FeCrAlY	FeCrAlY	FeCrAlY	Copper	Copper	Copper
Pore size (ppi)	10	10	30	10	30	60
Porosity	0.943	0.857	0.898	0.933	0.956	0.943
Thermal conductivity (k_s, W/mK)	26	20	20	310	300	320

analytical results are slightly smaller than those obtained from the experiments. This can be attributed to the simplification of the governing equations, i.e. the omission of axial thermal conduction in the energy equation and inertial term in the momentum equation, experimental errors, as well as the rather simplified comparison of experimental results for channel flow and analytical results for pipe flow. Comparison of analytical and experimental results for plain and metal-foam filled tubes (Fig. 15) also shows that the use of metal-foams greatly enhances heat transfer performance.

5. Conclusion

In this paper, the heat transfer performance of metal-foam filled pipes has been analyzed using the Brinkman-extended Darcy momentum model and the two-equation heat transfer model for porous media. Analytical solutions for temperature and velocity distributions have been carried out for constant heat flux boundary conditions. The effects of various metal-foam parameters on heat transfer have been examined. The results show that the overall Nusselt number of the metal-foam filled pipe increases with the increase of relative density (1-porosity) or pore density (ppi), especially when the thermal conductivity of the solid is much higher than that of the fluid. Although metal-foams with low porosity and small pore size (i.e. high pore density) are advantageous for achieving high heat transfer performance, pressure drop will be higher compared to that of plain tubes. It is also shown that for low Reynolds numbers the effect of the thermal conductivity of the foam on heat transfer is quite small and hence cheaper, low thermal conductivity foams can be used. When low thermal conductivity foams are employed the effect of pore density is quite small and thus high porosity foams can be used which will also lead to lower pressure drop. Compared to plain (hollow) tubes, the use of metal-foams can enhance heat transfer performance significantly, up to forty times.

Acknowledgements

This work is supported by the UK Engineering and Physical Sciences Research Council (EPSRC grant number: GR/T24364/01), National Basic Research Programme of China, (No. 2006CB601203), National Natural Science Foundation of China (No. 50576069), the Program for New Century Excellent Talents in University (NCET-04-0944), and Brief Award of Brunel University (WAE-DPA301). The authors also wish to thank the assistance of Mr. Ian Stirling, Porvair Plc., for providing the test samples.

Appendix A. General solutions of the partial differential equation

For the differential equation of form of

$$z^2 \cdot \frac{\partial^2 Y}{\partial z} + z \cdot p(z) \cdot \frac{\partial Y}{\partial z} + q(z) \cdot Y = 0 \tag{A.1}$$

which is one of the classical functions of mathematical physics [18]. One solution of this equation is: $f(z) = z^{\mu}\sum_{n=0}^{\infty} c_n z^n$. Assuming $p(z) = 1$ and $q(z) = -z^2$, dividing both sides by z^2 and simplifying, Eq (A. 1) takes the form

$$\frac{\partial^2 Y}{\partial z} + \frac{1}{z}\frac{\partial Y}{\partial z} - Y = 0 \tag{A.2}$$

which should be solved in this paper.

Based on the solution of (A. 1) the solution of (A. 2) is

$$J_0(z) = \sum_{n=0}^{\infty} \frac{1}{(n+v)!n!}\left(\frac{1}{2}z\right)^{2n}. \tag{A.3}$$

A second solution of Eq. (A. 1) is

$$f(z) = C \cdot J_0(z)\ln(z) + z^{\mu_2}\sum_{n=0}^{\infty} d_n(z) \cdot z^n.$$

Applying this to Eq. (A. 2) we get

$$Y_0(z) = J_0(z)\ln\left(\frac{1}{2}z\right) + \sum_{n=0}^{\infty} \frac{F_n}{(n+1)!(n+1)!(n+1)}\left(\frac{1}{2}z\right)^{2n+2}, \tag{A.4}$$

where, $F_n = \frac{n+1}{n}F_{n-1} - 1$ and $F_0 = -1$.

Therefore, the $J_0(z)$ and $Y_0(z)$ are two solutions for Eq. (A. 2).

For $J_1(z) = J_0'(z)$, and $Y_1(z) = Y_0'(z)$, $J_1(z)$ and $Y_1(z)$ can be determined as

$$J_1(z) = \left(\frac{1}{2}z\right)\sum_{n=0}^{\infty} \frac{1}{(n+v)!n!}\left(\frac{1}{2}z\right)^{2n} \tag{A.5}$$

$$Y_1(z) = J_1(z)\ln\left(\frac{1}{2}z\right) + \frac{1}{2}\sum_{n=0}^{\infty} \frac{1}{n!n!}\left(\frac{1}{2}z\right)^{2n-1} + \frac{1}{2}\sum_{n=0}^{\infty} \frac{F_n}{(n+1)!(n+1)!}\left(\frac{1}{2}z\right)^{2n}. \tag{A.6}$$

Accordingly, the form of the solutions, $(z \cdot J_1(z))' = z \cdot J_0(z)$ and $(z \cdot Y_1(z))' = z \cdot Y_0(z)$ can be obtained.

References

[1] A. Bhattacharya, V.V. Calmidi, R.L. Mahajan, Thermophysical properties of high porosity metal foams, International Journal of Heat and Mass Transfer 45 (2002) 1017–1031.
[2] K. Boomsma, D. Poulikakos, On the effective thermal conductivity of a three-dimensionally structured fluid-saturated metal foam, International Journal of Heat and Mass Transfer 44 (2001) 827–836.
[3] V.V. Calmidi, Transport phenomena in high porosity fibrous metal foams, Ph.D. thesis, University of Colorado, 1998.
[4] V.V. Calmidi, R.L. Mahajan, Forced convection in high porosity metal foams, Journal of Heat Transfer 122 (2000) 557–565.
[5] C.Y. Zhao, T. Kim, T.J. Lu, H.P. Hodson, Thermal Transport Phenomena in Porvair Metal Foams and Sintered Beds, Ph.D. report, University of Cambridge, 2001.
[6] C.Y. Zhao, T.J. Lu, H.P. Hodson, Natural convection in metal foams with open cells, International Journal of Heat and Mass Transfer 48 (2005) 2452–2463.

[7] M.S. Phanikumar, R.L. Mahajan, Non-Darcy natural convection in high porosity metal foams, International Journal of Heat and Mass Transfer 45 (2002) 3781–3793.
[8] A. Bejan, Convection Heat Transfer, second ed., Wiley, New York, 1995.
[9] R.M. Fand, T.E. Steinberger, P. Cheng, Natural convection heat transfer from a horizontal cylinder embedded in a porous medium, International Journal of Heat and Mass Transfer 29 (1986) 119–133.
[10] K. Vafai, C.L. Tien, Boundary and inertia effects on flow and heat transfer in porous media, International Journal of Heat and Mass Transfer 24 (1981) 195–203.
[11] C.Y. Zhao, T.J. Lu, Analysis of microchannel heat sinks for electronics cooling, International Journal of Heat and Mass Transfer 45 (2002) 4857–4869.
[12] S.J. Kim, D. Kim, D.Y. Lee, On the local thermal equilibrium in microchannel heat sinks, International Journal of Heat and Mass Transfer 43 (2000) 1735–1748.
[13] R. Nazar, N. Amin, D. Filip, I. Pop, The Brinkman model for the mixed convection boundary layer flow past a horizontal circular cylinder in a porous medium, International Journal of Heat and Mass Transfer 46 (2003) 3167–3178.
[14] C.Y. Zhao, T. Kim, T.J. Lu, H.P. Hodson, Thermal transport in high porosity cellular metal foams, Journal of Thermophysics and Heat Transfer 18 (n3) (2004) 309–317.
[15] D.Y. Lee, K. Vafai, Analytical characterization and conceptual assessment of solid and fluid temperature differentials in porous media, International Journal of Heat and Mass Transfer 42 (1999) 423–435.
[16] N. Wakao, S. Kaguei, T. Funazkri, Effect of fluid dispersion coefficients in packed beds. Correlation of Nusselt numbers, Chemical Engineering Science 34 (1979) 325–336.
[17] A.A. Zukauskas, Convective heat transfer in cross-flow, in: S. Kakac, R.K. Shah, W. Aung (Eds.), Handbook of Single-Phase Convective Heat Transfer, Wiley, New York, 1987.
[18] N.M. Temme, Special Functions An Introduction to the Classical Functions of Mathematical Physics, Wiley, New York, 1996.